Interstitial Hydrogen in the Early-Transition-Metal Halides

Jeremy K. Burdett* and Gordon J. Miller

Contribution from the Department of Chemistry, The University of Chicago, Chicago, Illinois 60637. *Received October 10, 1986*

Abstract: Until recently, the ZrCl and ZrBr structure types were believed to be adopted by the Group 3 and many lanthanoid metals. More careful scrutiny of the diffraction data, however, revealed the presence of many kinds of interstitial species, mostly identified to be hydrogen and oxygen. Directed synthetic strategies now can control the amount of interstitial, and it seems that these Group 3 species are not stable as binary halides. We examine the orbital nature of these binary systems concluding primarily that "GdCl" represents a Jahn-Teller type instability that is stabilized not by a geometrical distortion but by accomodating interstitial main group species. We then discuss the effects of hydrogen occupation in the various voids between the layers of metal atoms. Although the other main group atoms are more effective in their orbital interactions with the ZrCl-type framework, the net results are rather similar to the effects of hydrogen.

The early transition-metal halides are rich in structural examples based upon the octahedral metal clusters, M_6X_8 and M_6X_{12}.[1] These materials include isolated metal octahedra, e.g., Nb_6I_{11},[2] Nb_6Cl_{14}[3] as well as octahedra condensed into chains, as found in Gd_2Cl_3,[4] $NaMo_4O_6$,[5] and layers, e.g., ZrCl[6] and ZrBr.[7] In many cases, especially for the Groups 3 and 4 transition metals, interstitial atoms ranging from main group atoms to transition metals occupy the octahedral and tetrahedral interstices.[8-10] Since the empty clusters are electron deficient, interstitial species stabilize the structure by introducing strong metal-interstitial interactions.

Such inserted nonmetal species are quite prevalent in the layered metal halides, MX, in which M represents Sc, Y, Zr, Hf, or many lanthanoids.[8] Originally suggested as binary metal halides, only the structures of ZrCl and ZrBr have been substantiated. The Group 3 and lanthanide metal halides are not stable as pure binary compounds but contain significant concentrations of interstitial hydrogen, carbon, or oxygen, to name a few. Of particular interest are the hydride halides of the lanthanides, $LnXH_n$, in which n varies from $\sim$0.6 to 2.0. Neutron diffraction data finds the hydrogens preferentially in the tetrahedral holes between adjacent layers of metals for n = 0.6-0.9.[11] At the upper phase boundary of $LnXH_n$ (n = 2), there are two hydrogen atoms occupying each octahedral hole, essentially in two opposite triangular faces as well as in every tetrahedral hole.

In this section we use the tight-binding approximation within Extended Hückel theory to examine the nature of the bonding in these and other layered halides.[12,13] We are interested in elucidating any electronic reasons for the stability of these compounds with respect to alternative structures of the metal-halide parent, such as the NaCl or NiAs types, which are observed for other "neighboring" systems in the periodic table.

Chemical Bonding and Stability of "GdCl". Before tackling the diverse problem of interstitial hydrides, we shall consider the electronic structure of the parent "GdCl" framework, which, in fact, is only known for ZrCl[6] and ZrBr.[7] The structure consists of Gd_2Cl_2 slabs connected via van der Waals interactions between adjacent layers of halides. Within each slab, there are four close-packed planes of atoms stacked as Cl-Gd-Gd-Cl in the sequence *AbcA*; see Figure 1. The local environment of each metal atom is a trigonal antiprism—three by halides and three by other metal atoms. This stacking sequence is retained for most of the interstitial hydrides while for other main group atoms, the sequence switches to *AbaB*. We examine the electronic structure of both "GdCl" alternatives in the following discussion.

Let us construct the energy bands for the *AbcA* slab of "GdCl" beginning with the frontier orbitals of a C_{3v} $GdCl_3$ fragment, used to mimic the ligand field about each metal atom. Figure 2 illustrates this fragment orbital diagram. The three levels near -7.8 eV (labeled a_1 and e) are derived from the t_{2g} set of orbitals for the "$GdCl_6$" octahedral complex whereas the e set at -7.1 eV arises from the e_g orbitals. With the reduced asymmetric coordination of the metal atom, there is also a low-lying a_1-Gd sp_z hybrid orbital, which becomes important within the solid.[14]

Upon condensation of these $GdCl_3$ fragments, we obtain a puckered 6^3 net with stoichiometry GdCl, **1**. Such *AB* networks

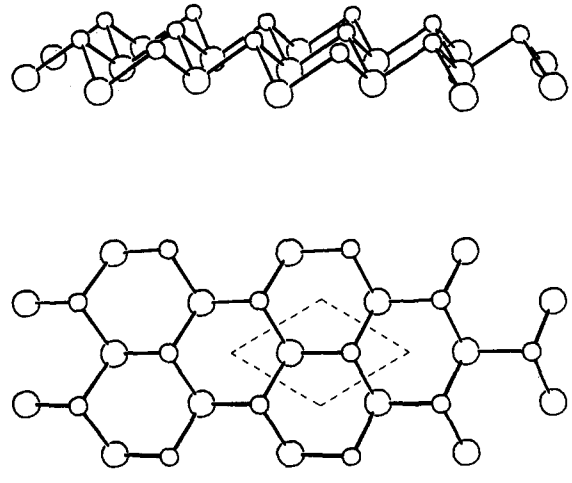

1

serve as important conceptual building blocks for several common structure types, e.g., zinc blende and rock salt to name only two. Because of the puckering, the two dimensional plane group of this layer is isomorphous to the point group C_{3v}, containing a threefold rotation axis and three mirror planes perpendicular to the lattice plane in addition to the translations. The importance of in-plane metal-metal bonding reveals itself in Figure 3 in which we illustrate the evolution of the Gd d and s levels from the isolated fragment to the orbitals at Γ for the condensed sheet with no

(1) Simon, A. *Angew. Chem.* **1981**, *93*, 23; *Angew. Chem. Int. Ed. Engl.* **1981**, *20*, 1.
(2) Simon, A.; von Schnering, H. G.; Schäfer, H. *Z. Anorg. Allg. Chem.* **1967**, *355*, 295.
(3) Simon, A.; von Schnering, H. G.; Wöhrle, H.; Schäfer, H. *Z. Anorg. Allg. Chem.* **1965**, *339*, 155.
(4) Lokken, D.; Corbett, J. D. *Inorg. Chem.* **1973**, *12*, 556.
(5) McCarley, R. E. *ACS Symp. Ser.* **1983**, *211*, 273.
(6) Adolphson, D. G.; Corbett, J. D. *Inorg. Chem.* **1976**, *15*, 1820.
(7) Daake, R. L.; Corbett, J. D. *Inorg. Chem.* **1977**, *16*, 2029.
(8) Simon, A. *J. Solid State Chem.* **1985**, *57*, 2.
(9) Ziebarth, R. P.; Corbett, J. D. *J. Am. Chem. Soc.* **1985**, *107*, 4571.
(10) Simon, A. In *Inorg. Solids*; Cheetham, A. K., Day, P., Eds.; Oxford University Press: in print.
(11) Mattausch, Hj.; Schramm, W.; Eger, R.; Simon, A. *Z. Anorg. Allg. Chem.* **1985**, *530*, 43.
(12) Bullett, D. W. *Inorg. Chem.* **1980**, *19*, 1780.
(13) Marchiando, J. F.; Harmon, B. N.; Liu, S. H. *Physica* **1980**, *99B*, 259.
(14) Albright, T. A.; Burdett, J. K.; Whangbo, M.-H. *Orbital Interactions in Chemistry*; Wiley: New York, 1985.

0002-7863/87/1509-4092$01.50/0

metal–metal interactions and, finally, to the sheet with all interactions included.

As the level scheme in Figure 3b attests, the ligand field is severely affected by the requirements of the translational subgroup. The d_{xz} and d_{yz} orbitals are found at −8.21 eV, the energy of the free atomic d orbitals, since there are no linear combinations of Cl s or p orbitals which transform similarly. The remaining Gd orbitals in this region are destabilized by the ligand field. When metal–metal interactions are turned on, the d_{z^2} and sp hybrid orbitals are greatly stabilized (~1.2–1.4 eV) as they are required to be in phase at Γ. For nodeless functions, e.g., s, p_z, and d_{z^2} orbitals, at each lattice site in a 3^6 net, the tight-binding energy band assuming nearest-neighbor interactions only is described by the expression

$$\epsilon(\mathbf{k}) = \alpha + 2\beta[\cos(\mathbf{k}a_1) + \cos(\mathbf{k}a_2) + \cos(\mathbf{k}(a_1 + a_2))] \quad (1)$$

in which α is the free orbital energy, and β is the resonance integral between adjacent orbitals. At the zone center, $\mathbf{k} = 0$, the energy, $\epsilon(\Gamma) = \alpha + 6\beta$, is the minimum of the band. On the other hand, the phase restrictions at Γ cause the $\{d_{x^2-y^2}, d_{xy}\}$ and $\{d_{xz}, d_{yz}\}$ sets to be destabilized as metal–metal overlap is included.

What is found at other points in the Brillouin zone? From a consideration of the phase relationships between adjacent unit cells, the only significant metal–metal bonding interaction involving Gd d_{z^2} and s functions occurs near Γ. We show the resulting crystal orbitals for the s-band at Γ, *K*, and *M* in **2**. At *K* and *M* in the

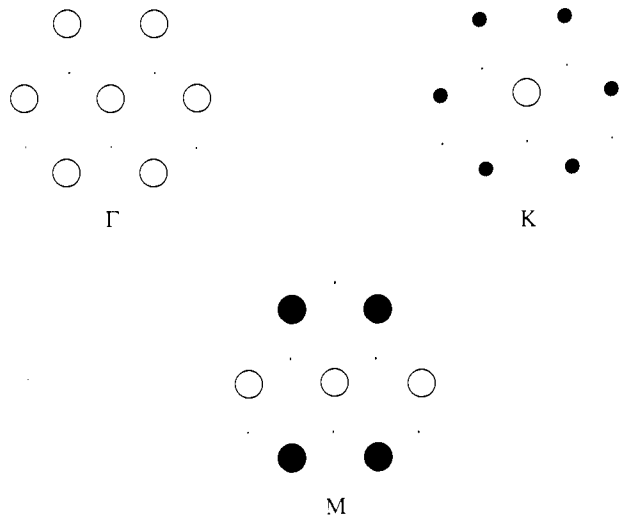

2

hexagonal zone, the resulting energies using eq 1 are $\epsilon(K) = -3\beta$ and $\epsilon(M) = -2\beta$. Also at these points, the degeneracies in the $\{d_{x^2-y^2}, d_{xy}\}$ and $\{d_{xz}, d_{yz}\}$ orbital sets are removed. The dispersion of these levels is controlled both by metal–metal and ligand field interactions. From the calculated electronic band structure for the puckered GdCl sheet shown in Figure 4, we see that a weak ligand field and strong M–M σ and π overlap (both imposed by the translational symmetry) result in low-lying $d_{x^2-y^2}$ and d_{xz} crystal orbitals. The other two levels (d_{xy} and d_{yz}) are destabilized by either a strong M–X interaction (d_{yz}) or M–M antibonding interactions (d_{xy}). Since the Γ*KM* direction possesses only the identity as its symmetry operation, these features in the Gd band arise via numerous orbital mixings and avoided crossings. In any case, with two metal–metal bonding levels at *K* and continuing on to *M*, the optimal electron count for maximizing the interaction between metal atoms is near d^3.

To complete the ZrCl-type "GdCl" slab, we need only to bring two such 6^3 puckered sheets together to form the *AbcA* sequence. Figure 5 illustrates three interaction diagrams involving the two sheets to form the slab at Γ, *K*, and *M* in the hexagonal zone. Each crystal orbital diagram is k-dependent since the wavefunctions at different wavevectors, **k**, are orthogonal, $\langle\psi_{\mathbf{k}'}|\psi_{\mathbf{k}}\rangle = \delta(\mathbf{k}' - \mathbf{k} - \mathbf{K})$, in which **K** is a reciprocal lattice vector. These diagrams, however, are slightly deceiving because we represent each level

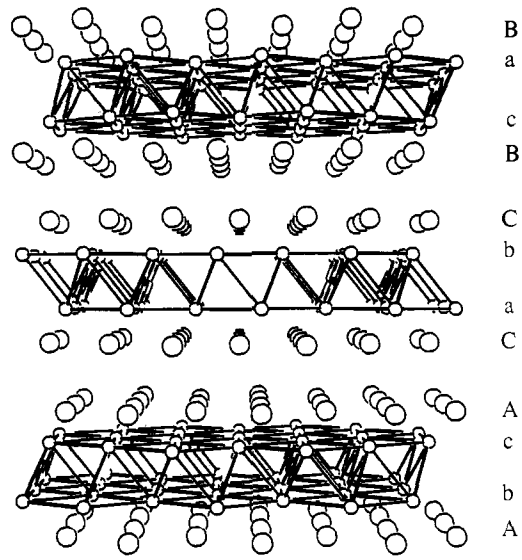

Figure 1. Perspective view of the ZrBr structure projected onto the (110) plane. Small circles are Zr; large circles are Br. A, B, and C indicate the stacking positions for each layer of atoms. In ZrCl, the four layer slabs are identical with those here; they are simply packed differently along the *c*-axis.

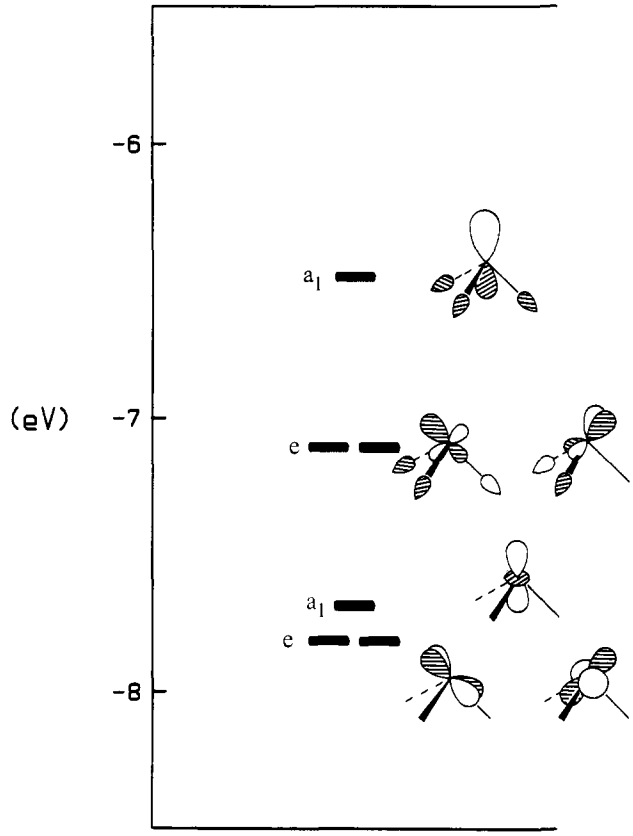

Figure 2. The frontier orbitals for the C_{3v} $GdCl_3$ fragment.

by a specific d or s orbital on the metal. At Γ and *K*, the isomorphous point group is C_{3v} while at *M* it is C_s which results in substantial mixing of orbitals with similar irreducible representations. Nevertheless, we indicate that orbital making the most significant contribution at each energy. Those orbitals containing s and p_z components have the largest interaction energies since their overlap integrals are largest. However, we see the effects of the halide ligand field at the points *K* and *M*, at which the intraplane Gd 6s crystal orbital has a higher energy than its free atom value, since the interlayer 6s–6s interaction does not quite stabilize the symmetric combination of these orbitals into the region containing intralayer bonding levels. In addition, we point

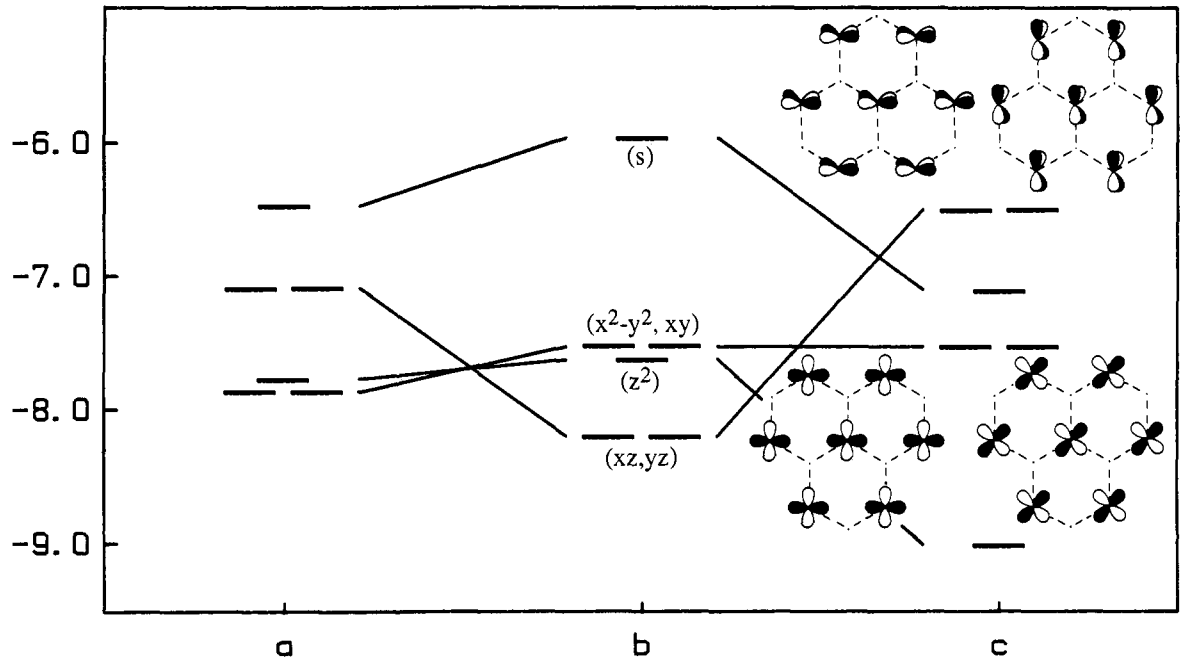

Figure 3. Evolution of the $GdCl_3$ frontier orbitals from the isolated fragment to the condensed 6^3 sheet, "GdCl": (a) the isolated fragment, (b) the condensed sheet without Gd–Gd interactions, and (c) the sheet with Gd–Gd interactions turned on.

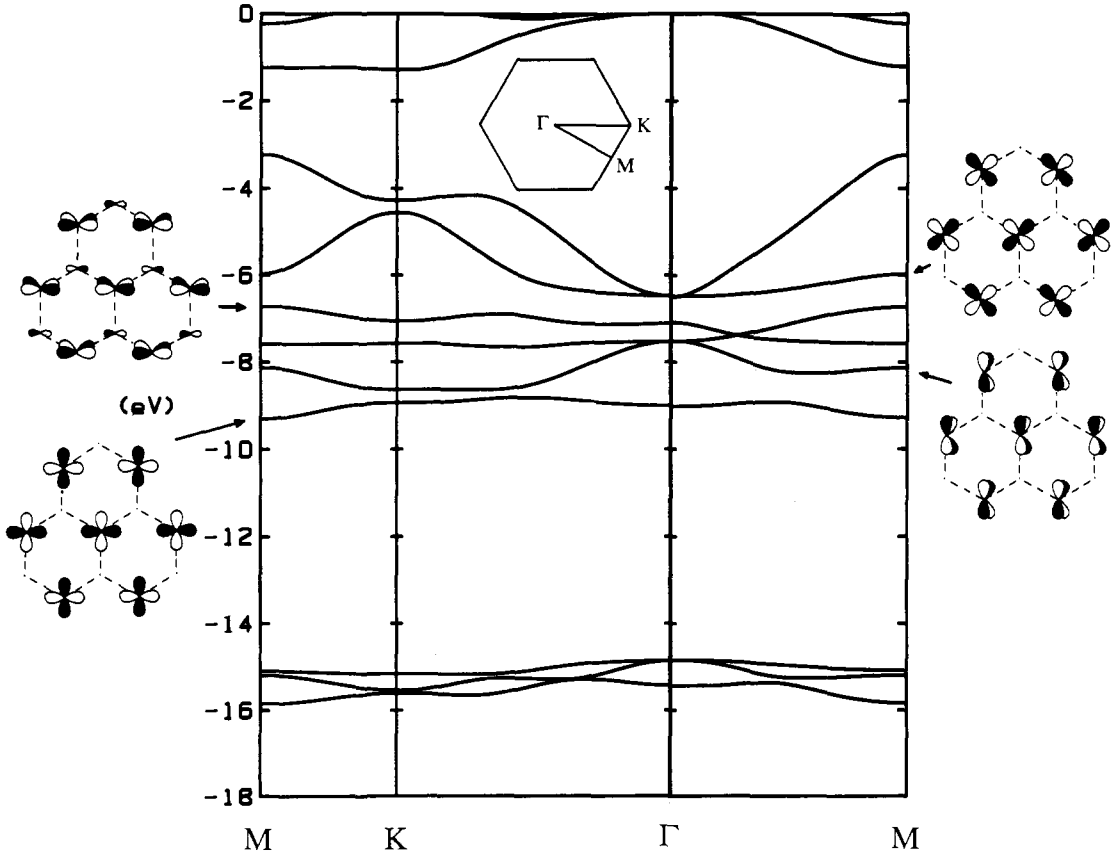

Figure 4. The calculated electronic band structure for the single sheet of "GdCl". The crystal orbital representation include those atomic orbitals on each metal which have the dominant component.

out the importance of these levels in shaping the bottom of the conduction band. At K and M we find the in-phase combination of $d_{x^2-y^2}$ and d_{xz} orbitals (plus the π-bonding d_{z^2} orbital) the most stabilized; both of these energy positions are due to their intralayer interactions (see Figure 4). These two M–M bonding levels are depicted in **3**.

The computed band structure as well as the total density of states (DOS) is shown in Figure 6 with the Fermi levels appropriate for d^2 and d^3 marked. The Fermi level for d^3 systems, e.g., ZrCl, lies below the π^* combination of d_{z^2} orbitals at Γ. On the other hand, the DOS at the Fermi level, $N(\epsilon_F)$, for d^2 is fairly large suggesting that if GdCl or any isoelectronic compound could be attained, it may have superconducting properties. However, this large $N(\epsilon_F)$ also indicates a certain degree of instability which may be alleviated by either a geometrical distortion (similar to a first-order Jahn–Teller effect) or by introducing interstitial species. The geometrical perturbation will cause the degeneracy at ϵ_F to separate, thereby stabilizing the new structure.[15] The

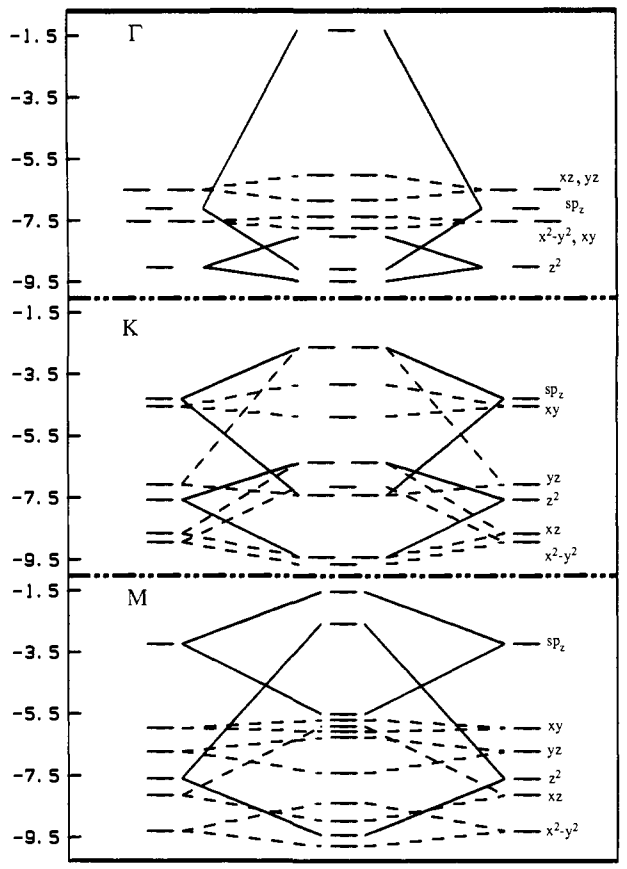

Figure 5. Crystal orbital interaction diagrams at the high symmetry points Γ, *K*, and *M* in the hexagonal Brillouin zone between two single "GdCl" sheets to form GdCl in the ZrCl slab structure. Solid lines indicate interactions involving the sp_z and d_{z^2} orbitals while the dashed lines indicate interactions concerning d_{xz}, d_{yz}, d_{xy}, and $d_{x^2-y^2}$ orbitals.

classic examples concern the "octahedral" complexes of d^9 Cu^{II} in which a tetragonal distortion of the octahedron separates the

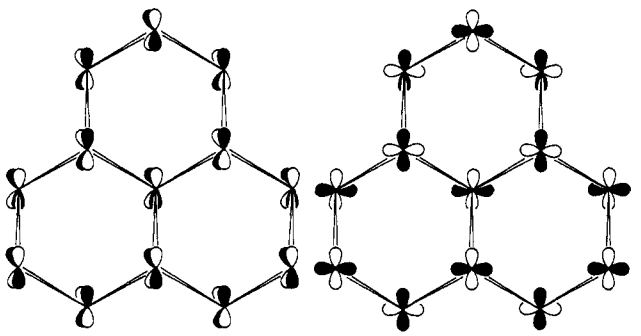

3

e_g set of levels into two nondegenerate orbitals.[15] Alternatively, interstitials may not split the degeneracy if they occupy a site of high point symmetry but will stabilize the structure by donating or accepting charge from the parent. Usually changes in the geometrical parameters of the host material accompany this charge transfer. A pedagogically interesting molecular example involves assembling methane from an H_4 tetrahedral cluster and an "interstitial" carbon atom. The schematic interaction diagram is shown in **4**. We note that neutral H_4 has two electrons in the t_2 orbital—a Jahn–Teller instability. Bonding and antibonding combinations are formed between the C p orbitals and the H_4 t_2 level which, upon filling the levels with eight electrons, removes the asymmetric occupation of the t_2 level in H_4. Furthermore, any interactions between the hydrogens are now repulsive, and, thus, the cluster has broken up into four ligands. We shall address

(15) Burdett, J. K. *Molecular Shapes*; Wiley: New York, 1980.

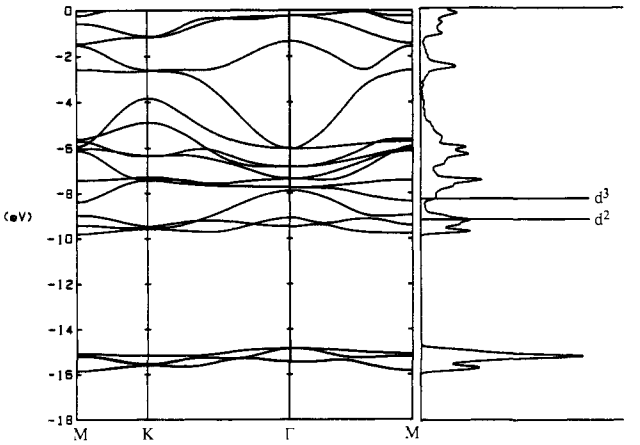

Figure 6. The electronic band structure and total DOS for GdCl in the ZrCl structure. The Fermi levels are indicated for electron counts d^2 (GdCl) and d^3 (ZrCl).

the question of interstitial interactions later in the chapter with the hydride halides.

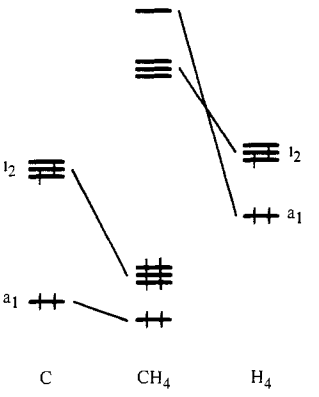

4

The structures of ZrCl and ZrBr are interesting in their own right, specifically because they are unique to the early transition-metal halides, as the NbO structure is unique to NbO.[16] Certainly the most common structure types for compounds with this range of electron counts include NaCl and NiAs, both of which contain octahedrally coordinated metal atoms and six-coordinate "anions"; octahedral in NaCl-type and trigonal prismatic in NiAs-type. What are the electronic properties of the ZrCl structure that favor its occurrence for the Group 4 metals? Certainly metal–metal bonding is important since we can express the stacking of adjacent atomic layers in ZrCl as *ABBA* as opposed to *ABAB* for NaCl and NiAs. As the orbital interaction diagrams in Figure 5 show, when the metal band in the puckered 6^3 MX sheet is partially occupied, interlayer M–M contacts, both π and σ type, enhance its stability. What does a detailed orbital picture convey about these three structures? For closed shell, eight electrons per formula unit, that structure which stabilizes the halogen p band most will be favored. Both NaCl and NiAs structures are preferred over ZrCl due to the larger coordination around the anion. In addition, NaCl is the most energetically favored at these counts since the nonbonded repulsions between the cation orbitals are smaller in the octahedron than in the trigonal prism thereby stabilizing the Cl p orbitals to a greater extent. As the metal-centered conduction band becomes occupied, however, the reduced coordination of the metal atom tends to favor the ZrCl structure type. With each Zr atom being three-coordinate, its "e_g-derived" σ^* levels (recall Figure 2) are stabilized relative to the octahedral complex and become more effectively involved in metal–metal interactions than those from NaCl or

(16) Bowman, A. L.; Wallace, T. C.; Yarnell, J. L.; Wenzel, R. G. *Acta Crystallogr.* **1966**, *21*, 843.

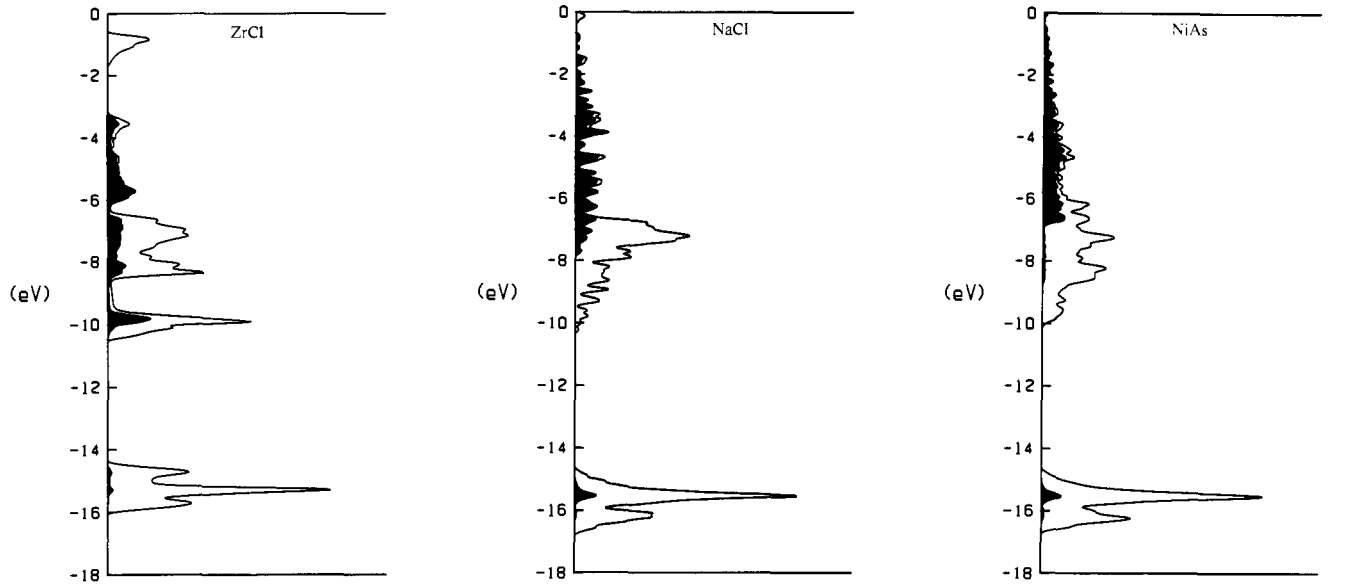

Figure 7. The total DOS and the e_g projection (shaded) for ZrCl in the ZrCl, NaCl, and the NiAs structure types, respectively. The shaded areas show the hydrogen atom contribution.

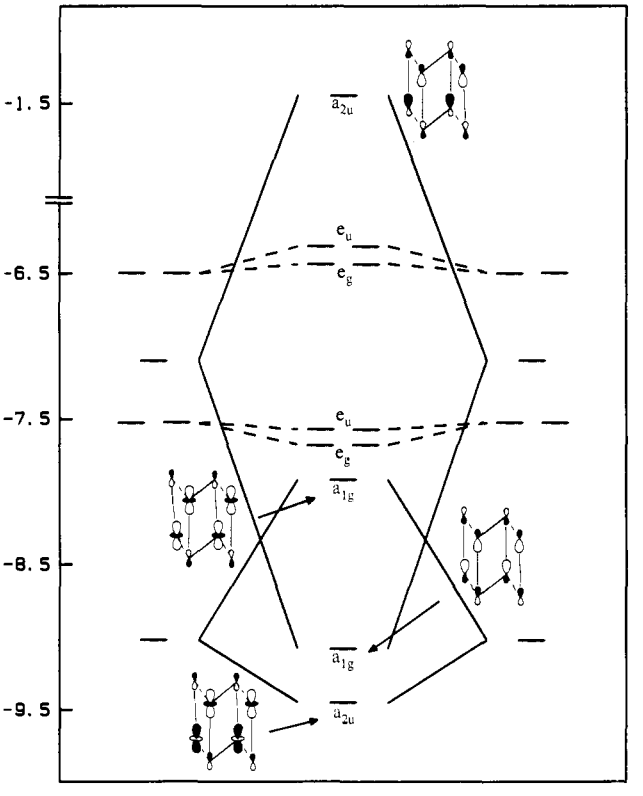

Figure 8. The crystal orbital interaction diagram at Γ between two single "GdCl" 6^3 sheets to form the "GdCl" slab structure in an *AbaB* stacking sequence. The labels correspond to D_{3d} point symmetry.

NiAs. This effect is nicely represented in the e_g projection of the total DOS for ZrCl, NaCl, and NiAs shown in Figure 7, in which we find a degree of e_g component at the bottom of the conduction band in ZrCl but not any in either NaCl or NiAs. Thus, we see two factors contributing to the stabilization of the ZrCl structure with respect to the NaCl structure: the through-space interaction (Figure 5) of metal orbitals and the symmetry-controlled mixing of "e_g" levels into the "t_{2g}" set.

These are familiar arguments for the electronic stability of NbO as well. Since ZrCl and NbO are isoelectronic, one may wonder about the specificity of structure for these two compounds. An important aspect to the electronic nature of NbO is the Nb–O π interaction which promotes both square-planar oxygen and Nb.[17]

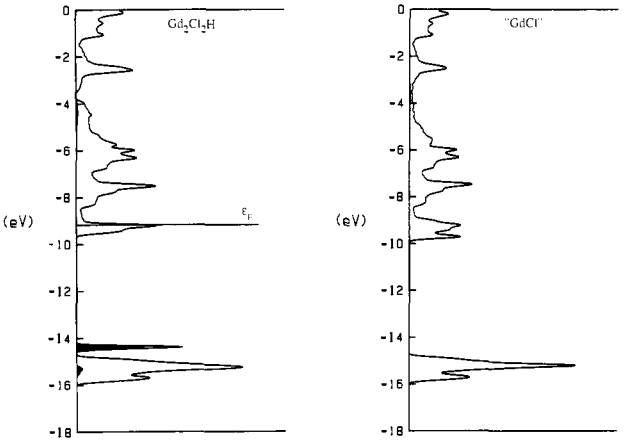

Figure 9. The total DOS diagrams for the Gd_2Cl_2H structure with the H atoms in the octahedral holes and parent GdCl framework. The shaded projection is the H band, and the Fermi level for the 21 electron is marked.

For the heavier main-group elements, π-bonding becomes much less prevalent relative to σ-bonding as pyramidal geometries become more significant. Therefore, combining these π-overlap arguments with a considerable matrix effect of the heavier halogens as compared to oxygen, it is unlikely that ZrCl will adopt the NbO structure. We should mention, however, that both structures involve condensation of M_6 octahedral clusters; M_6X_{12} for NbO and M_6X_8 for ZrCl. Previous treatments have shown their analogy to these clusters.[8,18]

Another important question concerns the comparison between NiAs and ZrCl, since the NiAs-type or some variant exist for several isoelectronic chalcogenides and pnictides. No binary halides, however, are known. The relative electronegativities seem to be crucial in sorting these two types. Since atoms with larger electronegativities prefer sites of low-coordination numbers, we find the ZrCl-type. Our calculations for the Cl Mulliken charge for NaCl, NiAs, and ZrCl as a function of d count (Table I) corroborate this point. Except for a few isolated examples, structural sorting diagrams, e.g., ones constructed by Pettifor, separate the NaCl and NiAs types rather well by using a Mendeleev number for each constituent.[19] The ZrCl structure type fits nicely into a gap within the NaCl structure block.

(17) Burdett, J. K.; Hughbanks, T. *J. Am. Chem. Soc.* **1984**, *106*, 3101.
(18) Schäfer, H.; von Schnering, H. G. *Angew. Chem.* **1964**, *20*, 833.
(19) Pettifor, D. *New Scientist* **1986**, 48.

Table I. Mulliken Charges on Cl in "GdCl" with the ZrCl-, NaCl-, and NiAs Structure Types

no. e⁻	q_{Cl}(ZrCl)	q_{Cl}(NaCl)	q_{Cl}(NiAs)
16	7.32	6.70	6.70
18	7.35	6.71	6.72
20	7.37	6.74	6.75
22	7.38	6.76	6.78

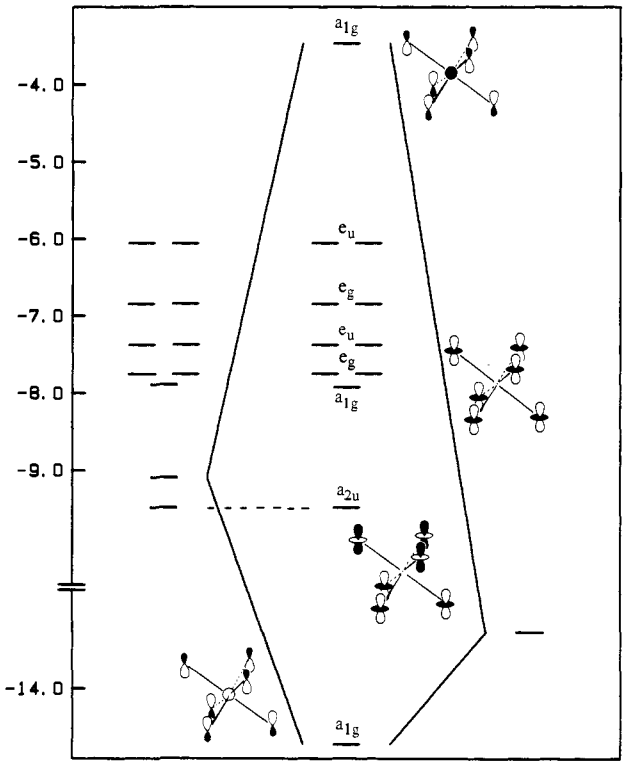

Figure 10. Crystal orbital interaction diagram at Γ for the GdCl framework and the H atoms in the octahedral holes. Note the shift in energy scale. The Fermi level for Gd_2Cl_2H occurs near the a_{2u} level.

One final issue before addressing the problem of interstitials remains to be examined: *AbcA* vs. *AbaB* stacking of atomic layers within the slab. In accord with the observed structures of ZrCl and ZrBr, the preference is for the *AbcA* sequence based upon our computational results. The alternative *AbaB* sequence adjusts the ligand field around the metal atoms from three coordinate to a C_{3v}-distorted tetrahedron. In fact, this double layer stacking is observed in the Al–Si network of $CaAl_2Si_2$[20] as well as for PtTe.[21] Zheng et al. have examined the electronic structure in $CaAl_2Si_2$ in some detail,[22] so we need not further elaborate them here. We shall discuss in orbital terms, however, why this stacking variant is not observed in the early transition-metal halides. The interaction diagram between the two puckered 6^3 GdCl sheets at Γ in Figure 8 reveals the effects of ligand field destabilization and the metal–metal interactions. The Gd–Gd π bonding a_{2u} orbital suffers from Gd–Cl σ* interactions between Gd and its second nearest-neighbor Cl atoms, as does the a_{1g} level. On the other hand, the d_{z^2} a_{1g} orbital is destabilized primarily by π* overlap between metals while there is a σ-bonding interaction with Gd d_{z^2} and the second nearest-neighbor Cl p_z orbital. Within *AbcA* stacking, the same metal–metal interactions are found as in *AbaB*, but the ligand field involving second nearest-neighbors is considerably reduced. The only ligand field adjustments that stabilize the Group 3 metals involve interstitials like oxygen which serve as electron sinks, oxidizing the metal to 3+, e.g., YClO. In the next section, we discuss the effects of less severe interstitials, hydrogen atoms, for stabilizing these transition-metal halides.

The Interstitial Hydrogen Atom. Interstitial hydrogen atoms provide rather specific structural and electronic problems to study. Neutron diffraction allows reasonably accurate determination of hydrogen atom positions in materials for which X-rays would not provide definitive results although the method suffers from requiring large sample sizes.[23] Concerning the electronic properties of transition-metal hydrides (we shall not consider *covalent* materials, e.g., silanes), most exhibit metallic conductivity, and many are nonstoichiometric. The character of the metal–hydrogen interaction, whether it is *metallic* or *ionic*, is usually controversial and certainly blurs the distinction between "hydrogen solid solutions" and "hydrides".[24] Within the framework of molecular orbital theory, the H 1s orbital is the consummate σ-donor model since it contains no angular nodal planes. For interstitial hydrogens, only a very restricted number of cluster or crystal orbitals can interact with the totally symmetric 1s orbital. Consequently, for the series of hydride–halides, $LnXH_n$, only the in-phase combination of fragment orbitals from the two 6^3 puckered sheets may participate in bonding/antibonding interactions with the interstitial. In the following discussion, we examine the electronic effects on the parent MX structure by the occupation of the various interstices between the metal layers.

Gd_2Cl_2H (Octahedral Holes). Since there is one octahedral hole for every lattice site in any close-packed arrangement of atoms, this stoichiometry results when every octahedral interstice between two adjacent layers of Gd atoms is occupied by hydrogen. Neutron diffraction data have located the hydrogen atoms in tetrahedral voids for compounds of this type as well as for Group 3 and 4 binary hydrides (with the fluorite structure).[24] ZrClH and $TbClH_2$ have two hydrogens per octahedral hole, but these are nearly coplanar with two opposite triangular faces. Octahedral coordination of H is known in HNb_6I_{11},[25] $HCsNb_6I_{11}$,[26] and the alkali hydrides which adopt the NaCl structure and, then, only confirmed for LiH and NaH by using diffraction techniques.[27]

As a possible alternative interstitial, however, we illustrate the total DOS for this Gd_2Cl_2H structure and compare it with the DOS of its parent GdCl framework in Figure 9. Since the H 1s orbital will preferentially interact only with those crystal orbitals in GdCl which are totally symmetric about each octahedral hole, the features of the DOS between the two structures have few differences. The hydride band shows essentially no dispersion at −14.4 eV. It is also clear from the appearance of the conduction bands for both compounds that the major M–H interactions occur in the M–M bonding region of the "GdCl" DOS. Since the H atom lies quite near the nodal plane of the Gd d_{z^2} orbital, the primary overlaps occur with Gd s and p_z functions, as shown in the energy level diagram of Γ in Figure 10. The peak at the Fermi level for Gd_2Cl_2H (21 electrons) is essentially the antisymmetric combination of Gd d_{z^2} orbitals between adjacent planes, as indicated in Figure 10, which has π-bonding characteristics. Also, the bottom of the conduction band for the interstitial structure is destabilized slightly from its congener in the parent "GdCl". This arises from the crystal orbital at *M* in GdCl which has the

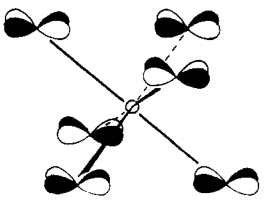

5

(20) Gladyshevskii, E. I.; Kipyakevich, P. I.; Bodak, O. I. *Ukr. Fiz. Zh. (Russ. Ed.)* **1967**, *12*, 447.
(21) Bhan, S.; Gödecke, T.; Schubert, K. *J. Less Common Metals* **1969**, *19*, 121.
(22) Zheng, C.; Hoffmann, R.; Nesper, R.; von Schnering, H. G. *J. Am. Chem. Soc.* **1986**, *108*, 1876.
(23) Bacon, G. E. *Neutron Diffraction*, 3rd ed.; Oxford University Press: London, 1975.
(24) Goldschmidt, H. J. *Interstitial Alloys*; Plenum Press: New York, 1967.
(25) Simon, A. *Z. Anorg. Allg. Chem.* **19678** *355*, 311.
(26) Imoto, H.; Corbett, J. D. *Inorg. Chem.* **1980**, *19*, 1241.
(27) Wells, A. F. *Structural Inorganic Chemistry*, 5th ed.; Oxford University Press: London, 1984.

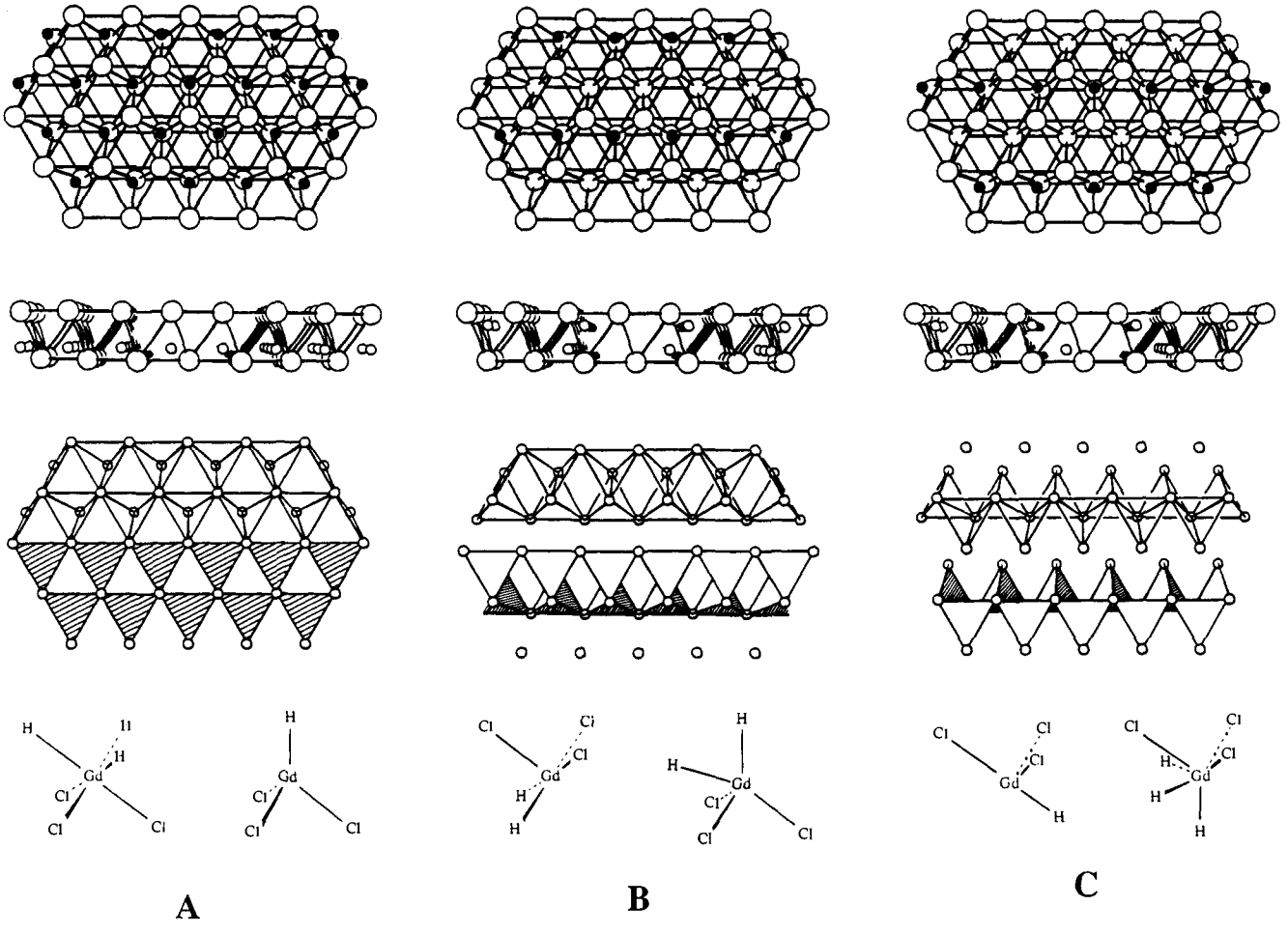

Figure 11. Three ways of occupying one-half of the tetrahedral holes in the GdCl framework to obtain Gd_2Cl_2H. In the top views, the shaded circles represent H, some of which are hidden by the top sheet of metal atoms in B and C. The polyhedral drawings indicate which interstices are occupied.

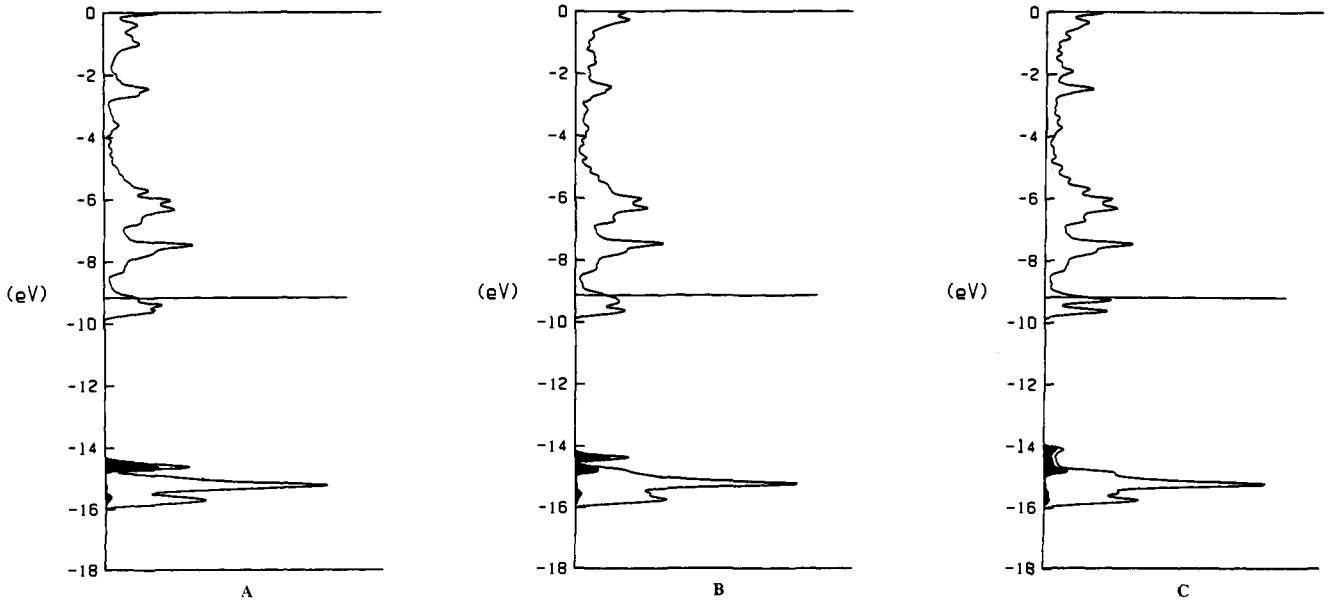

Figure 12. The total DOS for each of the three interstitial structures A, B, and C, respectively. The darkened portions are the hydrogen projections of the total DOS.

appropriate symmetry characteristics imposed by the phase factors for interacting with the hydride, **5**. We note that the d orbitals on the waist of each M_6 octahedron form a symmetric combination.

On the basis of our earlier arguments regarding the stability of GdCl and ZrCl, occupation of each octahedral void by H does not stabilize the Group 3 halides. One electron reduction of this Gd_2Cl_2H alternative places the Fermi level in a region of the conduction band similar to ϵ_F for ZrCl. The Gd–H overlap population, however, remains unchanged and rather weak (0.086) for both electron counts. This relatively weak Gd–H bonding interaction certainly suggests substantial hydrogen mobility at this stoichiometry and a degree of difficulty in locating the H atom at these centers.

Gd_2Cl_2H (Tetrahedral Holes). With the number of tetrahedral holes equal to twice the number of octahedral voids, the stoi-

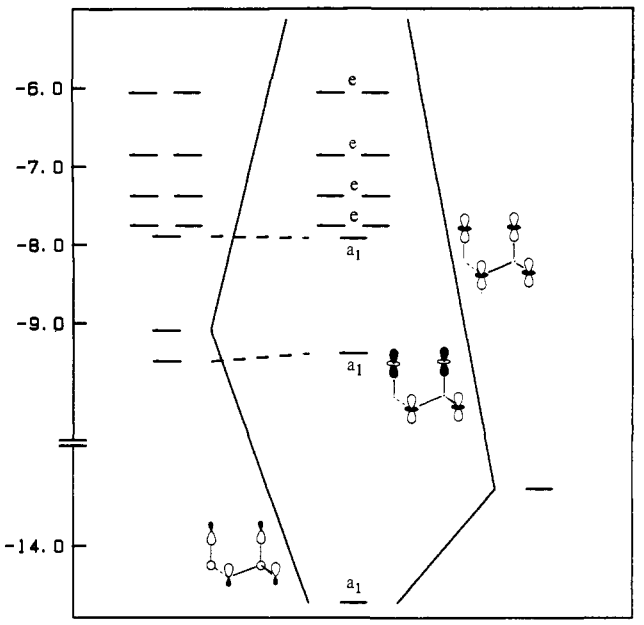

Figure 13. Crystal orbital interaction diagram at Γ between the GdCl framework and H atoms in one-half of the tetrahedral holes. The Fermi levels appropriate for Gd_2Cl_2H are indicated in each plot.

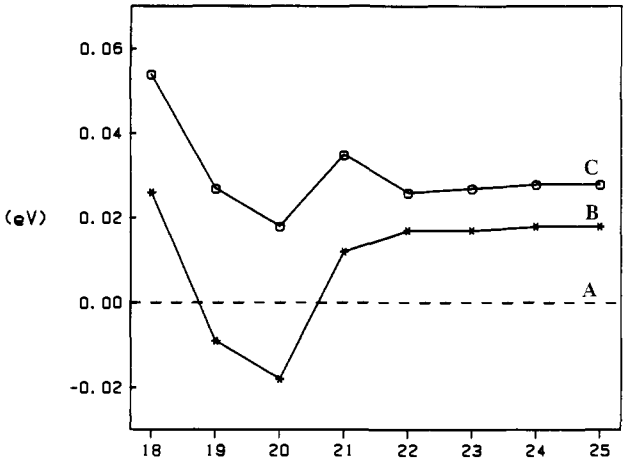

Figure 14. Energy difference curves comparing the total energy of the three tetrahedral interstitial alternatives A, B, and C as a function of electron count. The reference structure is chosen as A.

chiometric ratio 2:2:1 indicates only half occupancy of these sites. There exist an infinite number of ways of accomplishing this, but we restrict examination only to those which involve the smallest orthohexagonal cell in the parent GdCl framework: the three patterns in Figure 11 (labeled A, B, and C). Since each Cl is three coordinate to Gd and each H atom is four coordinate, the average coordination number of Gd is five. A maintains the threefold rotation axis with one layer of Gd atoms surrounded by a tetrahedron and the other by a trigonal antiprism of ligands (both hydrogens and halides). B and C have orthorhombic symmetry in the plane. In B one set of Gd atoms are "square pyramidal" while the other set are "trigonal bipyramidally" coordinated, certainly in an idealized sense. Finally, we find rather unusual coordination modes in case C: a bicapped tetrahedron for one-half the Gd atoms and a distorted four-coordinated sawhorse for the others. These coordination environments at each metal are also indicated in the figure.

The total DOS curves for each type are shown in Figure 12. There are noticeable differences in the features associated with the hydrogen band as well as near the bottom of the conduction band among the three plots. To a large degree, however, the three DOS curves are quite similar especially in the halide region as well as the majority of the Gd conduction band—a consequence

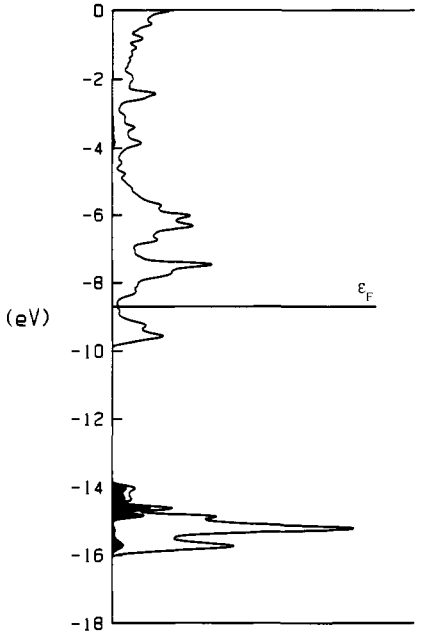

Figure 15. The total DOS for the compound $GdClH_{0.75}$ in which H occupies tetrahedral holes. The Fermi level, ϵ_F, for this electron count is marked. The shaded areas show the hydrogen atom contribution.

of the symmetry requirements for the H 1s orbital. The interactions between the interstitial hydrogen atom and the GdCl framework at Γ for case A are shown in Figure 13. Since occupation of these tetrahedral holes removes all symmetry operations in the lattice plane, e.g., the twofold rotation axes, the bands are classified under the group C_{3v}. The largest overlap involves the H 1s orbital with Gd s and p_z components, thereby removing one of the metal–metal bonding bands in GdCl to the top of the Gd s,d-manifold. As in ZrCl one of the e orbitals at Γ (the $d_{x^2-y^2}$ level) becomes stabilized at other regions in the Brillouin zone so that the Fermi level for 22 electrons lies just below the M–M π^* type a_1 level. This analysis remains similar for cases B and C as well although the trigonal symmetry is removed.

We can account for the differences in the three DOS plots by examining the distribution of hydrogens in the tetrahedral voids. For case A, there is one H atom per unit cell, and the ordering of occupied holes maximizes the distance between all hydrides. As seen from Figure 12a, a single sharp hydride peak occurs at −14.5 eV. The peak shape arises from the weak interaction of the H 1s orbital with the d orbitals of the basal plane of the tetrahedron from angular overlap considerations. In the orthorhombic structure B, we observe the interstitials in adjacent edge-sharing tetrahedra. The hydride peak now splits into two corresponding to the symmetric and antisymmetric combination of H 1s orbitals (a twofold axis lies in the lattice plane perpendicular to the H–H vector). The peak splitting at the bottom of the conduction band is slightly obscured by the omnipresent e band that becomes stabilized. This feature in the DOS for this orthorhombic alternative indicates that case A will be energetically favored at d^0 counts (this nonbonded repulsion argument is an MO analogy to electrostatic repulsion between like ions), but for initial nonzero d-counts, alternative B will becomes relatively more stable since there is a lower M–M interlayer bonding band associated with those metal atoms weakly interacting with the hydrogen. The energy difference curve for these two systems, Figure 14, bears out this prediction although all ΔE values are rather small. For the electron count appropriate for Gd_2Cl_2H, we calculate a slightly negative energy "barrier" (−0.06 eV) for interconversion between A and B along the path of least action suggesting rather mobile H atoms at these concentrations. The third structural variant, C, produces a dispersive hydride band arising from the chains of edge-sharing metal tetrahedra stuffed with hydrogen: note the one-dimensional character of the H

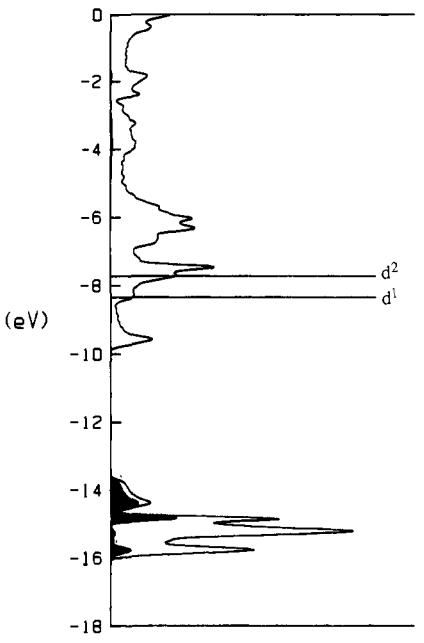

Figure 16. Total DOS of GdClH with the H atoms occupying every tetrahedral hole. The shaded region is again the H projection, and the Fermi levels are indicated for d^1 (GdClH systems) and d^2 (ZrClH systems).

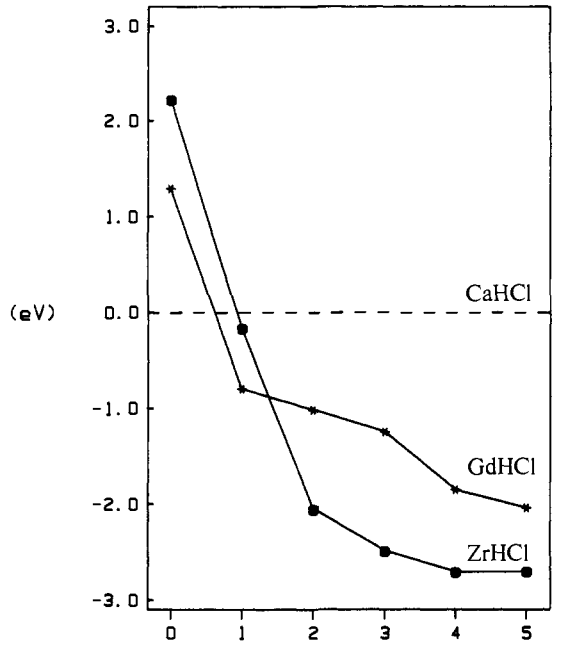

Figure 17. Energy difference as a function of d electron count for the GdClH-type and ZrClH-type structures against the CaClH structure. CaHCl is preferred at d^0, GdClH at d^1, and ZrClH at d^2.

projection of the total DOS. The features inherent in its energy difference curve are explained with the same reasoning as applied to B, although its closed shell repulsions increase its relative total energy for d^0 counts and, thereby, affect its relative energy at later counts.

Concerning the stability of $GdClH_{0.5}$, again we find that $N(\epsilon_F)$ is rather large. More electron-rich systems seem more likely to occur. It is reasonable, therefore, for the hemihydrides of the Group 3 and lanthanide halides to accept further hydrogen interstitials as in the compounds $LnXH_{0.7\text{-}0.9}$.[11] Figure 15 shows the DOS for an idealized structure of $GdClH_{0.75}$ in which the Fermi level lies in the midst of a low density of states—the band again corresponds to the same e band indicated in ZrCl (Figure 5).

For the documented compound $ZrBrH_{0.5}$, the observed structure is distorted to orthorhombic symmetry although the H atom positions have not been accurately determined.[28] Since the calculated Fermi level for 23 electrons occupy levels which are M–M antibonding in all three cases, it is possible that the hydrogen atoms are displaced away from the center of the tetrahedral hole in order to stabilize a M–M bonding band into the occupied region.

GdClH (Tetrahedral Holes). When every tetrahedral interstice is occupied in the GdCl framework, this 1:1:1 stoichiometry results. The heavy atoms remain stacked in the sequence *AbcA* as the hydrogens form a slightly puckered 6^3 net between the metal atom layers—an arrangement similar to the carbon skeleton in graphite. The qualitative orbital characteristics of such a net are discerned in the hydride projection of the total DOS for GdClH in Figure 16. The DOS of the p_z band in graphite, the prototypic 6^3 network, has a characteristic shape and is well-documented.[29] The π^* region is easily seen in the hydride projection, but the π region is contracted to a sharp peak due primarily to avoided crossings with the Cl p bands. With both tetrahedral holes occupied, the two interlayer M–M bonding levels in "GdCl" are destabilized near the top of the conduction band, and, so, the Fermi level for d^1 species, like GdClH, falls just below the π^* d_{z^2} band at Γ. Furthermore, as suggested from this electron count and the absence of d_{z^2} contributions, only one M–M bonding band remains—again the stabilized e component. Therefore, our pervading stability arguments imply that such a structure is a possible alternative for GdClH, although there are no conclusive reports for any Group 3 or lanthanoid compound.

The documented structure for ZrBrH is rather different.[30] Here, every octahedral hole is occupied by two hydrogen atoms, each lying close to the centers of opposite triangular faces. Furthermore, the stacking sequence of the heavier atoms has rearranged to *AbaB*. Computations on the two alternatives predict this sequence to be energetically favored, a consequence of the greater two-center four-electron repulsions between the "anionic" hydride and the halides in the *AbcA* type. Another known MXH structure type is the CaClH arrangement[27] (PbClF type) in which a rocksalt arrangement of CaCl has been tetragonally distorted as shown in **6** and followed by H occupation of all tetrahedral

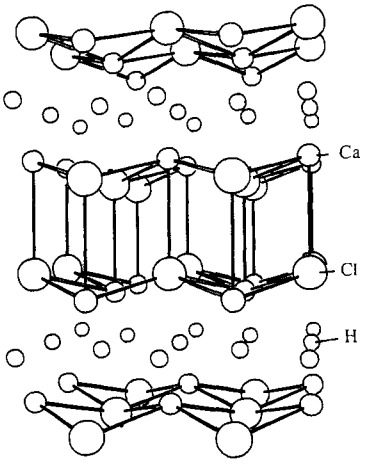

6

holes between two adjacent layers of metal atoms (large circles, Cl; medium circles, Ca; and small circles, H). The diagram emphasizes the relationship to the parent NaCl structure, although the shortest M–X distances parallel to the *c*-axis occur between atoms on opposite sides of the H layer. Although the number of examples for each case is limited, the CaHCl type is observed for

(28) Marek, H. S.; Corbett, J. D.; Daake, R. L. *J. Less Common Metals* **1983**, *89*, 243.
(29) Burdett, J. K. *Prog. Solid State Chem.* **1984**, *15*, 173.
(30) Wijeyesekera, S. D.; Corbett, J. D. *Solid State Commun.* **1985**, *54*, 657.

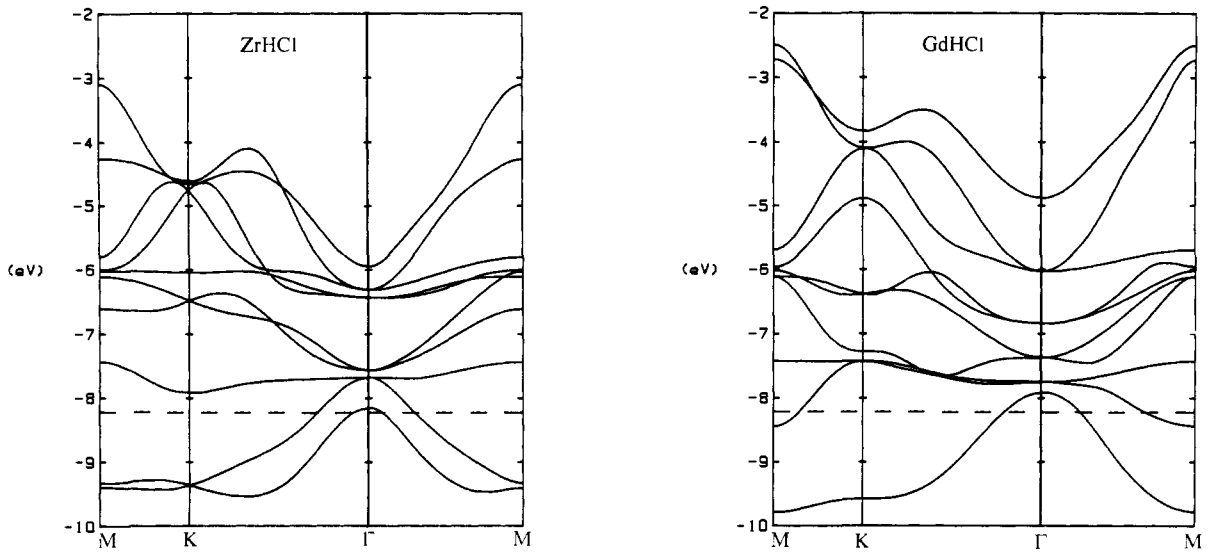

Figure 18. Energy band structures in the metal region for both GdClH and ZrClH. The dashed lines in both diagrams mark the d orbital energy for the free metal atom. At Γ, the lowest metal level is M–M π^* in both cases.

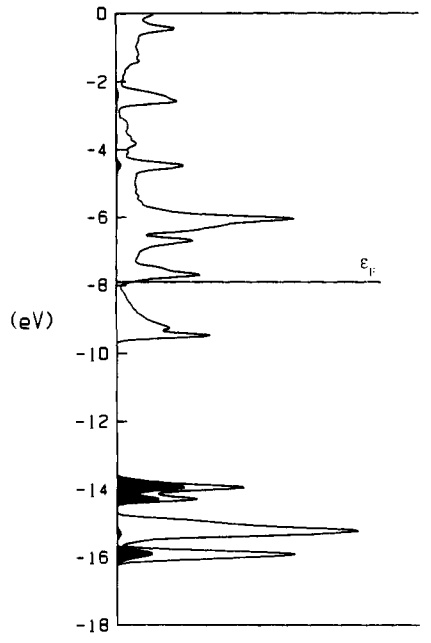

Figure 19. The total DOS for the ZrClH structure. The darkened area is the H projection, and the Fermi level is indicated for the electron count appropriate for ZrClH.

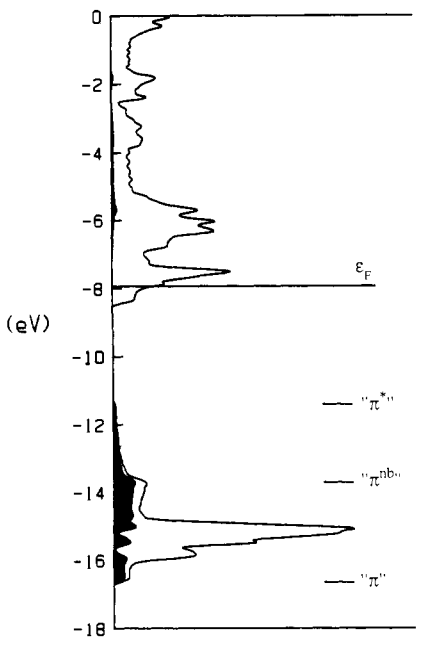

Figure 20. The total DOS for the hypothetical interstitial hydride, $GdClH_{1.5}$. The three levels correspond to the H levels at Γ and are labeled according to the π system in the allyl molecule. Again, the shaded area is the H band, and the Fermi level is indicated for $GdClH_{1.5}$.

d^0 metals, the GdClH type for d^1, and the ZrBrD type for d^2. The results of Extended Hückel calculations on these three structure types correctly predict this trend as noted from the energy differences curves in Figure 17.

The CaHCl is favored only for d^0 metals arises from reasoning similar to understanding the preference of NaCl over ZrCl at d^0 counts. The greater ligand field strength of the distorted square-pyramidal geometry causes the e_g derived bands to become less involved in metal–metal bonding than in the GdClH-type structure. Furthermore, the hydrides are arranged so that the t_{2g} set feels a substantial ligand field as well as in **7**. Compared

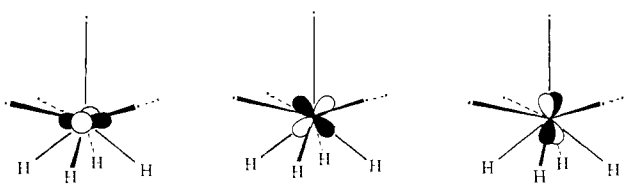

7

to the orbitals of GdClH and ZrClH, therefore, the Cl and H bands in CaHCl are more stabilized while the Gd conduction band is more destabilized.

We differentiate between GdClH and ZrBrH by noticing that two low-lying metal–metal bonding bands are found for the ZrBrH structure whereas only one exists for GdClH, as shown by the energy band structures in these regions in Figure 18. For both cases, one component of the e band at Γ is stabilized at other points in the zone, contributing predominantly to this low-lying band. Since it contains mostly $d_{x^2-y^2}$ and d_{xy} character (the xy plane is parallel to the two-dimensional lattice), the metal–metal bonding band in GdClH is more stable than in ZrClH, because the hydrides in tetrahedral holes have a smaller overlap with these orbitals than those in the nearly trigonal planar voids. The second metal–metal bonding band in ZrClH occurs because the H 1s orbital interacts only with the basal lobes of the Gd d_{z^2} orbital and not with the more extensive axial lobe (as is the case for the hydride in GdClH). The ZrClH structure, therefore, is energetically favored for d-counts above d^1. Also, as seen from its DOS in Figure 19, the

location of the Fermi level for ZrBrH confirms again our stability arguments.

$GdClH_{1.5}$. Occupation of all tetrahedral voids and additional occupation of all available octahedral holes results in this formula. Of the Group 3 and rare-earth hydride halides thus far reported, the relative stoichiometric ratios jump from 1:1:1 to 1:1:2 (M:X:H). By filling these three sites, a wide hydride band emerges as seen in the DOS curve of Figure 20. Adjacent to the DOS we indicate the three levels at Γ which have a large hydride component. Understanding the hydride band is analogous to understanding the π system in the three carbon allyl system except that we now have three adjacent *layers* of atoms. The relative phases of the hydride orbitals at Γ correspond to the usual splitting pattern in the allyl system and are labelled as such in the figure, intimating that the hydrogen–hydrogen interaction is not negligible.

On the basis of the position of ϵ_F for the 23-electron compound, we can extract an electronic reason that such compounds may not materialize. The octahedral hydride removes the M–M band which was observed in the GdClH structure—the same effect was observed in Gd_2Cl_2H (octahedral hole). We find ϵ_F, therefore, above the energy for the free atom d orbitals and just above a M–M π^* level at Γ. In retrospect, we find at this stoichiometry that the three metal–metal bonding bands for the ZrCl structure[12] have been completely removed from the bottom of the conduction band due to metal–hydrogen interactions. The H atoms in the tetrahedral sites have more effective overlap with the sp_z hybrid and d_{z^2} orbitals whereas the H atoms in the octahedral holes interact with the e band we have previously mentioned. In a sense, the orbital interactions are "saturated", but we have an extra half an electron per formula unit.

$GdClH_2$. As the final example, we turn to these extremely hydride-rich phases. Reported for $TbClH_2$,[31] the heavier atoms in this structure exhibit an *AbaB* sequence while each tetrahedral hole is occupied by H and each octahedral void by two H atoms as in ZrBrH. From the location of the Fermi level for 24 electrons on the total DOS in Figure 21, we confirm the nonmetallic nature of this compound. Again we find that electrostatic arguments support the observed stacking sequence since this arrangement minimizes repulsions between the halides and the hydrides in the "trigonal" holes. Because the halides lie over the tetrahedral holes between the metal layers, the top of the valence band is mostly derived from these hydride orbitals due to the closed shell repulsions. The bottom of the conduction band is mostly M–M π bonding between the antisymmetric combination of d_{z^2} orbitals in adjacent layers but weakly antibonding within the sheets. From the ligand field destabilization, however, these levels are above the free atom d orbital energy value, and, therefore, it is unlikely that chemical substitution or intercalation will be possible in this closed-shell compound.

Aspects of Other Interstitial Species. As opposed to interstitial hydrogen atoms, the other main group elements have p orbitals accessible for interaction with the metal halide conduction band. Of the reported structures, the larger carbides occupy octahedral voids, e.g., Sc_2Cl_2C and Zr_2Cl_2C,[32] whereas oxygen atoms are found in the tetrahedral holes, YClO.[33] Nitrogen atoms occur in octahedral holes in the layered material Zr_2Cl_2N[32] but in tetrahedral sites in the one-dimensional compound Gd_2NCl_3.[8] Figure 22 illustrates the total DOS for the interstitial carbide and oxide, respectively, which portrays the general features inherent in all of these main group interstitial compounds.[34] The valence band is comprised mostly of the interstitial p orbitals lying above the halide p band. Certainly, the position of this band in the spectrum depends upon the electronegativity of the interstitial as witnessed in YClO. The shape of the conduction band, on the other hand, depends upon the specific site that is occupied. Recall from our previous hydride analysis that the octahedral interstice effectively interacted with the $d_{x^2-y^2}$ orbital (one of the e bands), whereas the orbitals in the tetrahedral sites overlap mostly with the d_{z^2} and sp_z hybrid orbitals on the metal. In both Sc_2Cl_2C and YClO, the bottom of the conduction band is M–M bonding and lies below the d orbital energy for the free atom. Therefore, it is possible to introduce electron density into this band either via chemical substitution, i.e., Zr_2Cl_2C[32] or Zr_2Cl_2N[32] or by intercalation, Li_xYClO.[33]

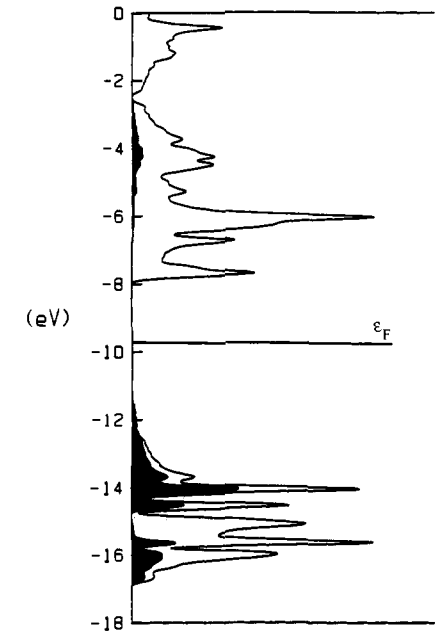

Figure 21. The total DOS for $GdClH_2$. The shaded areas show the hydrogen atom contribution.

Unlike the hydrides, however, the stacking sequence of the heavy atoms is *AbaB* and not *AbcA*, as found in ZrCl and $LnXH_{0.7-0.9}$. For the interstitial carbides of these two alternatives, the metal atom is "octahedrally" coordinated in *AbaB* stacking while trigonal prismatically coordinated in the other. The correlation between the closed-shell repulsions between anionic orbitals and the preference for octahedral coordination for d^0 and d^1 metals provide a sound argument for finding the *AbaB* sequence in both SC_2Cl_2C and Zr_2Cl_2C. Figure 23 illustrates the DOS for M_2X_2C in the alternative sequence. A small gap opens for d^2 systems—a plausible alternative for Nb_2Cl_2C, or is it? The COOP curves[35] for the metal–metal interactions in Figure 24 reveal that the interlayer forces are significantly antibonding just below the Fermi level for d^2 although the intraplane overlaps are bonding in nature. This band is predominantly the symmetric combination of M d_{z^2} orbitals which have π^* character. Even M–C interactions are antibonding in this band. The gap occurs in the DOS from the ligand field effects of the trigonal prismatic coordination and not due to any second-order Jahn–Teller effects which normally stabilize a series of bands. Since NbCl or any intercalates have not been successfully synthesized, we question the thermodynamic stability of this interstitial carbide.

As a final remark, we would like to point out some similarities between the interstitial hydrides and the more halogen-rich Group 3 and lanthanoid halides. One example, in particular, is the orthorhombic alternative for Gd_2Cl_2H, case B in Figure 11. If we consider the M–M linkages which surround those octahedral holes that are farthest from the interstitial hydrides, we find that this network of "bonds" is an edge-sharing chain of M_6 octahedra, as found in Gd_2Cl_3. It is certainly noteworthy that replacing H^- by Cl^- reproduces this formula. Now, for two chloride ions to occupy adjacent tetrahedral holes in the GdCl framework, an enormous distortion would ensue. The chains of edge-sharing

(31) Mattausch, Hj.; Simon, A.; Ziebeck, K. *J. Less Common Metals* **1985**, *113*, 149.
(32) Hwu, S.-J.; Ziebarth, R. P.; Winbush, S. V.; Ford, J. E.; Corbett, J. D. *Inorg. Chem.* **1986**, *25*, 283.
(33) Ford, J. E.; Corbett, J. D. *Inorg. Chem.* **1985**, *24*, 4120.
(34) Ziebarth, R. P.; Hwu, S.-J.; Corbett, J. D. *J. Am. Chem. Soc.* **1986**, *108*, 2594.
(35) Hughbanks, T.; Hoffmann, R. *J. Am. Chem. Soc.* **1983**, *105*, 3528.

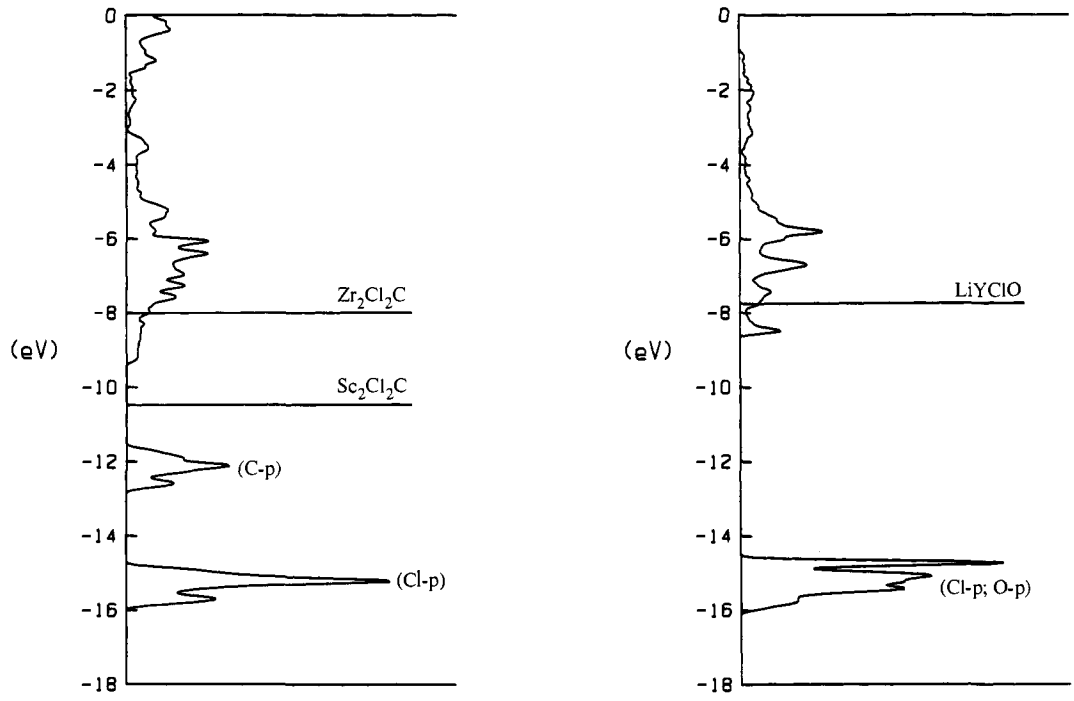

Figure 22. The total DOS for the Sc_2Cl_2C and YClO structures, respectively. The Fermi levels for Sc_2Cl_2C, Zr_2Cl_2C, and LiYClO are indicated.

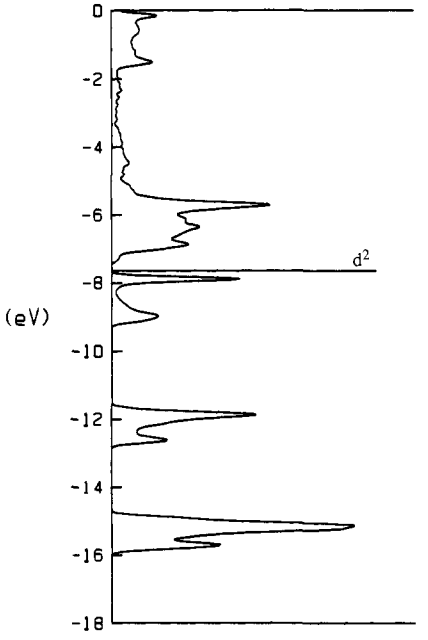

Figure 23. The total DOS for the Sc_2Cl_2C alternative structure.

Table II. Parameters for Extended Hückel Calculations

	orb	H_{ii} (eV)	$\zeta_1(c_1)^a$	$\zeta_2(c_2)^a$
Gd	6s	−7.67	2.14	
	6p	−5.01	2.08	
	5d	−8.21	3.78 (0.7765)	1.381 (0.4587)
C	2s	−21.4	1.625	
	2p	−11.4	1.625	
Cl	3s	−24.2	2.36	
	3p	−15.0	2.04	
H	1s	−13.6	1.30	
O	2s	−32.3	2.28	
	2p	−14.8	2.28	

[a] Exponents: double-ζ d functions are used for transition metals. No f-orbital functions were included for Gd.

octahedra, however, would remain intact. This suggests the possibility of producing compounds derived from breaking up the ZrCl layer structure into cluster fragments based upon some of

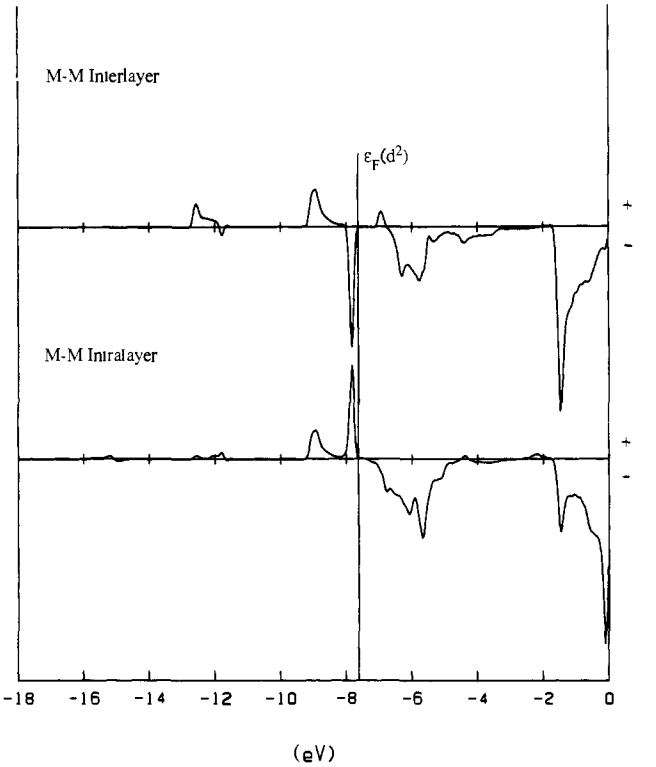

Figure 24. The COOP curves for interlayer and intralayer metal–metal interactions in the alternative Sc_2Cl_2C structure: +/− indicates bonding/antibonding interactions.

the known hydrides.[36] Also, by using known halogen-rich materials, we may deduce the interstitial site occupancy of hydrogen in a variety of hydride halides.

Summary

In this section we have discussed in orbital terms the importance of interstitial species, specifically H, in stabilizing the ZrCl framework for Group 3 and lanthanoid metals. For the ZrCl

(36) Berroth, K.; Simon, A. *J. Less Common Metals* **1983**, *76*, 41.

structure, the bottom of the conduction band contains three metal-metal bonding levels. For d^3 systems like ZrCl, these bands are completely occupied, whereas for d^2 counts, obviously they are not. Instead of geometrically distorting, interstitial hydrides enter the gaps between adjacent metal atom layers and interact in specific ways with the metal orbitals depending upon the sites they occupy. The effects of other main group atom interstitials are not significantly different.

Acknowledgment. The research was supported by NSF DMR 8414175 and DMR 8216892.

Appendix

All of the calculations described in this paper used the Extended Hückel method[37] both for the molecular orbital calculations of the fragment and for the tight-binding computations on the crystalline solids. The atomic parameters are listed in Table II.

The following geometrical parameters were used: (1) all M-M distances were set at 3.82 Å where appropriate; (2) all M-Cl distances were set to 2.81 Å; (3) the interstitial atoms occupied the geometrical centers of each interstice based upon these distances. All lattice sums included third nearest-neighbor cells and were restricted to two dimensions in ZrCl-type phases and three-dimensions for NaCl-type, NiAs-type, and CaHCl phases. To produce the DOS and COOP curves, a special points set for the appropriate irreducible wedge of the Brillouin zone was selected.[38] A total of 64 points were used.

(37) (a) Hoffmann, R. *J. Chem. Phys.* **1963**, *39*, 1397. (b) Whangbo, M.-H.; Hoffmann, R. *J. Am. Chem. Soc.* **1978**, *100*, 6093. (c) Ammeter, J. H.; Bürgi, H.-B.; Thibeault, J. C.; Hoffmann, R. *J. Am. Chem. Soc.* **1978**, *100*, 3686.

(38) Pack, J. D.; Monkhorts, H. J. *Phys. Rev. B* **1977**, *16*, 1748.

Communications to the Editor

Direct Observation of a Mode-Selective (Non-RRKM) van der Waals Reaction by Picosecond Photofragment Spectroscopy†

David H. Semmes,‡ J. Spencer Baskin, and Ahmed H. Zewail*

Contribution No. 7555, Arthur Amos Noyes Laboratory of Chemical Physics California Institute of Technology Pasadena, California 91125

Received February 17, 1987

The idea of directing reactions by selectively exciting particular vibrational modes with lasers (laser-selective chemistry) has stimulated much experimental and theoretical research aimed at exploring its feasibility and the deviation from statistical RRKM behavior in large molecules. In the absence of collisions, the yield and rate of a reaction will be determined by the specific rate of intramolecular vibrational-energy redistribution (IVR) from the initial mode excited to the other modes in the molecule and by the rate of bond breaking (vibrational predissociation). If k_{IVR} is larger than k_{VP}, then the chemistry is from a statistically formed distribution of vibrational states and a statistical behavior (RRKM) may prevail, even if a laser is used to selectively excite the initial state of the reagent. It is this interplay between IVR and VP that determines the mode selectivity of the reaction. Excitation of the molecule with short enough pulses, short compared to k_{IVR}^{-1} and k_{VP}^{-1}, should allow us to view these processes in real time and hopefully establish conditions for nonstatistical behavior.

We report here the direct observation of mode-selective picosecond laser-induced photofragmentation for the reaction

$$\text{stilbene–He} \rightarrow \text{stilbene} + \text{He}$$

Real-time measurements of the reaction rates of the van der Waals molecule stilbene–helium are given as a function of *reagent* and *product* internal energies. We have observed a mode dependent, rather than energy dependent, unimolecular decay rate and a mode dependence in the rate of product formation up to an excess vibrational energy of four times the bond energy.

In picosecond photofragment spectroscopy[1] experiments, a picosecond pulse initiates the reaction in a molecular beam and, in general, a second picosecond pulse, delayed in time, monitors the nascent fragment. Here, the pulse excites the stilbene-type modes of the van der Waals (vdW) molecule (reagent), and the spectrally dispersed fluorescence of the reagent and product is time resolved on the picosecond time scale, as we reported earlier.[2] In this way, we can monitor the reaction dynamics from reagent state to product state.

The excitation spectra of *trans*-stilbene[3] and stilbene–He[4] have been published. Furthermore, the IVR dynamics of stilbene has been characterized,[3a] and recent work on the excitation spectra of the complex shows selective line broadening among the low-energy states.[4b] The stoichiometry of the complexes (1:1 or 1:2) has been determined by using sub-Doppler measurements of the rotational constants of the emitting species,[2,5] which allows us to positively distinguish between stilbene and stilbene–He spectra. We have studied the reaction when the reagent is excited to 83, 95, 198, and 396 cm^{-1} in the excited state (S_1) of the complex. These energies correspond to the vibrational modes 36^137^1, 37^2, 25^1, and 25^2, respectively, where the superscript indicates the number of quanta in the torsion (37) or in the bend (25) mode. The binding energy of He to stilbene in the excited state is determined to be less than 50 cm^{-1}.

To obtain the state distribution of the product, dispersed fluorescence spectra were measured at each excitation energy studied. For 37^2 reagent excitation, most of the fluorescence intensity is from vibrationless product stilbene (0^0); the rest is from the S_1 + 47 cm^{-1} state of stilbene (37^1). The fluorescence spectrum

†This work supported by a grant from the National Science Foundation. Some support was also provided by the President's Fund.

‡NSF predoctoral fellow.

(1) (a) Knee, J. L.; Khundkar, L. R.; Zewail, A. H. *J. Chem. Phys.* **1985**, *82*, 4715; (b) **1985**, *83*, 1996. (c) Knee, J. L.; Khundkar, L. R.; Zewail, A. H. *J. Phys. Chem.* **1985**, *89*, 4659. (d) Scherer, N. F.; Doany, F. E.; Zewail, A. H.; Perry, J. W. *J. Chem. Phys.* **1985**, *84*, 1932. (e) Scherer, N. F.; Knee, J. L.; Smith, D. D.; Zewail, A. H. *J. Phys. Chem.* **1985**, *89*, 5141 see also ref 13.

(2) Baskin, J. S.; Semmes, D. H.; Zewail, A. H. *J. Chem. Phys.* **1986**, *85*, 7488.

(3) (a) Syage, J. A.; Lambert, W. R.; Felker, P. M.; Zewail, A. H.; Hochstrasser, R. M. *Chem. Phys. Lett.* **1982**, *88*, 266. Syage, J. A.; Felker, P. M.; Zewail, A. H. *J. Chem. Phys.* **1984**, *81*, 4685, 4706. Felker, P. M.; Lambert, W.; Zewail, A. H. *Ibid.* **1985**, *82*, 3003. (b) Amirav, A.; Jortner, J. *Chem. Phys. Lett.* **1983**, *95*, 295. (c) Suzuki, T.; Mikami, N.; Ito, M. *J. Phys. Chem.* **1986**, *90*, 6431. (d) van Zee, R.; Zwier, T. S.; Spangler, L. H. *J. Phys. Chem.*, in press.

(4) (a) Zwier, T. S.; Carrasquillo, E. M.; Levy, D. H. *J. Chem. Phys.* **1983**, *78*, 5493. (b) Taatjes, C. A.; Bosma, W. B.; Zwier, T. S. *Chem. Phys. Lett.* **1986**, *128*, 127.

(5) (a) Baskin, J. S.; Felker, P. M.; Zewail, A. H. *J. Chem. Phys.* **1986**, *84*, 4708. (b) Baskin, J. S.; Felker, P. M.; Zewail, A. H. *J. Chem. Phys.* **1987**, *86*, 2483.

0002-7863/87/1509-4104$01.50/0